A stress-induced cilium-to-PML-NB route drives senescence initiation

Jinghua Hu (Hu.Jinghua@Mayo.edu)
Mayo Clinic

Xiaoyu Ma
Mayo Clinic

Yingyi Zhang
Mayo Clinic

Yuanyuan Zhang
shengjing hospital of China Medical University

Xu Zhang
Mayo Clinic https://orcid.org/0000-0002-9784-0481

Yan Huang
Mayo Clinic

Kai He
Mayo Clinic

Chuan Chen
Mayo Clinic

Jielu Hao
Mayo Clinic

Debiao Zhao
Mayo Clinic

Nathan LeBrasseur
Mayo Clinic https://orcid.org/0000-0002-2002-0418

James Kirkland
Mayo Clinic https://orcid.org/0000-0003-1676-4905

Eduardo Chini
Mayo Clinic https://orcid.org/0000-0003-1555-4834

Qing Wei
Shenzhen Institutes of Advanced Technology https://orcid.org/0000-0001-7803-1139

Kun Ling
Mayo Clinic https://orcid.org/0000-0002-2388-5492

Article

Keywords:

Posted Date: May 26th, 2022

DOI: https://doi.org/10.21203/rs.3.rs-1522828/v1

A stress-induced cilium-to-PML-NB route drives senescence initiation

Xiaoyu Ma[1], Yingyi Zhang[1], Yuanyuan Zhang[8], Xu Zhang[3], Yan Huang[1,2], Kai He[1], Chuan Chen[1], Jielu Hao[1], Debiao Zhao[1], Nathan K. LeBrasseur[3], James L. Kirkland[3], Eduardo N. Chini[2,3,4], Qing Wei[6,*], Kun Ling[1,*], Jinghua Hu[1,2,7,*]

[1]Department of Biochemistry and Molecular Biology, Mayo Clinic, Rochester, MN, USA.
[2]Mayo Clinic Robert M. and Billie Kelley Pirnie Translational Polycystic Kidney Disease Center, Mayo Clinic, Rochester, MN, USA.
[3]Mayo Clinic Robert and Arlene Kogod Center on Aging, Mayo Clinic, Rochester, MN, USA.
[4] Department of Anesthesiology, Mayo Clinic, Rochester, MN, USA.
[5]Department of Physiology and Biomedical Engineering, Mayo Clinic, Rochester, MN, USA.
[6]Center for Energy Metabolism and Reproduction, Institute of Biomedicine and Biotechnology, Shenzhen Institutes of Advanced Technology, Chinese Academy of Sciences (CAS), Shenzhen, China.
[7]Division of Nephrology and Hypertension, Mayo Clinic, Rochester, MN, USA.
[8]Department of Clinical Genetics, ShengJing Hospital of China Medical University, Shenyang, Liaoning, China.

*Co-corresponding authors
Correspondence: hu.jinghua@mayo.edu

Abstract

Cellular senescence contributes to tissue homeostasis and age-related pathologies. However, how senescence is initiated in damaged cells remains vague. Here, we discover that irreparable stresses induce transient biogenesis of cilia, which are used by stressed cells to directly communicate with the promyelocytic leukemia nuclear bodies (PML-NBs), the validated stress signaling hub, to initiate senescence responses. Mechanistically, a ciliary ARL13B-ARL3 GTPase cascade negatively regulates the association of transition fiber protein FBF1 and SUMO-conjugating enzyme UBC9. Irreparable stresses downregulate the ciliary ARLs to release UBC9, which SUMOylates FBF1 at the ciliary base. SUMOylated FBF1 then translocates to PML-NBs to promote PML-NB-dependent senescence initiation. Remarkably, *Fbf1* suppression effectively subdues global senescence burden and prevents associated health-span decline in irradiation-treated mice. Collectively, our findings assign primary cilia a central role in inducing senescence program and identify them as promising targets to dampen senescence-associated detrimental damage in future senotherapy strategies.

Introduction

Cellular senescence is a programmed response that healthy cells enter an irreversible growth-arrest and apoptosis-resistant state, established by constitutive activation of the $p16^{INK4a}$-RB and/or p53-$p21^{CIP1}$ pathways, when experiencing irreparable stresses[1,2]. Senescent cells secret excessive pro-inflammatory cytokines, chemokines, proteases, and growth factors, which are collectively known as the senescence-associated secretory phenotype (SASP)[1]. Senescence occurs throughout life and can be beneficial in tissue repair and homeostasis[3,4]. However, unchecked senescence results in deleterious SASP secretion that contributes to increased cancer risk and age-related diseases[3]. Genetic or pharmacological clearance of senescent cells effectively improves survival and/or healthspan in rodent models[5].

The promyelocytic leukemia nuclear bodies (PML-NBs) are proteinaceous nuclear structures with instrumental roles in regulation of various stress-induced responses including senescence[6,7]. The structural basis of PML-NBs is the PML protein, a tumor suppressor dynamically and functionally associated with hundreds of PML-NB components (also termed PML interactome)[8]. In response to stresses, the number, composition, size, and posttranslational modifications (e.g., SUMOylation, phosphorylation, and acetylation) of PML-NBs undergo significant changes[8]. However, molecular insights into stress-induced biogenesis and function heterogeneity of PML-NBs remain poorly understood.

Primary cilia evolve as sensory devices that protrude from most eukaryotic cell surfaces to convert environmental cues into diverse cellular signaling[9,10]. We discovered that irradiation (IR) induces robust but transient ciliogenesis in stressed cells. Further analyses revealed that transient ciliogenesis in stressed mammalian cells are accompanied by acute downregulation of two ciliary GTPases ARL13B and ARL3, and the opposite upregulation of a transient fiber (TF) component FBF1. ARL13B and ARL3 are mutated in Joubert syndrome[11,12]. ARL13B serves as a guanine nucleotide exchange factor (GEF) to activate ARL3[13,14]. Mechanistically, we discovered that the ARL13B-ARL3 GTPase cascade negatively regulates UBC9-mediated SUMOylation of FBF1 at the ciliary base. Irreparable stresses suppress ARLs expression and thus enhance FBF1 SUMOylation. SUMOylated FBF1 then translocates from the ciliary base to PML-NBs to promote stress-induced PML-NB upregulation and initiates senescence. Excitingly, genetic ablation of *Fbf1*

protects mice from IR-induced senescence propagation and associated frailty. Our study highlights a strategy to counteract senescence-associated pathologies.

Results

Transient ciliogenesis is essential for senescence initiation in IR-treated human cells

When studying IR-induced senescence in human fetal lung fibroblasts (IMR-90) cells, we observed transient but robust ciliogenesis, as evident by both ciliation ratio and cilia length, during the progression of senescence (Fig. 1a). To determine if primary cilia is required for senescence progression, we knocked down *IFT88,* which encoded an essential protein for ciliogenesis. *IFT88*-deficient IMR-90 cells showed impaired senescence initiation upon IR-treatment (Fig. 1b), supporting a critical role for primary cilia in regulating senescence. By screening dozens of ciliary proteins in IR-treated IMR-90 cells, we found that two ciliary ARL GTPases, ARL3 and ARL13B, both mutated in Joubert syndrome, was downregulated (Fig. 1c). In drastic contrast to ARL GTPases, we found FBF1, a transition fiber component at the ciliary base[15], was upregulated during senescence progression (Fig. 1c). Intriguingly, the moment that the level of ARLs and FBF1 change during senescence progression occurs after cilia form in stressed cells (Fig. 1a, c). These data suggest that there is an opposite regulation of the ciliary ARLs and TF component FBF1 during senescence progression in stressed cells.

ARL3 deficiency promotes senescence

To first confirm that ARL3 indeed regulates cellular senescence, we examined two primary cell models commonly used in senescence studies, IMR-90 cells and mouse embryonic fibroblasts (MEFs). Compared to IR-treated control cells, IR-treated *shARL3* IMR-90 cells exhibited significantly greater senescence responses characterized by β-galactosidase activity (Fig. 1d), molecular senescence markers (Fig. 1e), and expression of SASP genes (Fig. 1f). Similarly, *Arl3*$^{-/-}$ MEFs consistently exhibited much higher senescence responses than control cells after IR treatment (Supplementary Fig. 1a-d). Meanwhile, we established CRISPR/Cas9-engineered *ARL3*$^{-/-}$ renal collecting tubule epithelia (RCTE) cell lines. *ARL3*$^{-/-}$ RCTE cells consistently exhibited much higher senescence responses than wildtype cells after IR treatment (Supplementary Fig. 1e-g). Consistently, IR-treated *ARL3*$^{-/-}$ cells were resistant to apoptosis (Supplementary Fig. 1f, h). Intriguingly, the protein expression of ARL3 is strongly inhibited upon induction of senescence in all mammalian cells tested (Fig. 1e and Supplementary Fig. 1c, f). Collectively, our data demonstrate that ARL3 acts as a negative regulator of senescence in mammalian cells.

ARL13B recapitulates the role of ARL3 in senescence regulation

As with ARL3, *ARL13B*-knockdown IMR-90 cells (Fig. 1g-i), or *ARL13B*$^{-/-}$ RCTE cells (Supplementary Fig. 1i-k), exhibited greatly enhanced senescence responses than control cells after IR treatment, suggesting that Joubert syndrome GTPases ARL13B and ARL3 likely act in the same genetic pathway to regulate senescence. This observation is in consistent with the fact that ARL13B acts as a GEF to activate ARL3[13,14].

FBF1 promotes cellular senescence

In accord with the drastic upregulation of FBF1 in senescent cells, FBF1 deficiency suppressed senescence responses (Fig. 2a-c), enhanced apoptosis (Fig. 2d) and reduced viability (Fig. 2e) in IR-treated s*hFBF1* IMR-90 cells. Studies in MEFs isolated from *Fbf1*$^{tm1a/tm1a}$ mutant mice[16] further supported that FBF1 deficiency led to compromised senescence induction (Supplementary Fig. 2a, b) and reduced viability (Supplementary Fig. 2c) after IR-treatment. We then established CRSPR/Cas9-engineered *FBF1*$^{-/-}$ RCTE cell lines. Consistently, *FBF1*$^{-/-}$ RCTE cells recapitulated the phenotypes of s*hFBF1* IMR-90 cells in IR–induced senescence (Supplementary Fig. 2d-f). Remarkably, overexpression of FBF1 alone in normal IMR-90 cells further enhanced senescence responses after IR treatment (Fig. 2f-h). Together, these results highlight that the level of FBF1 plays a decisive role in driving senescence initiation in mammalian cells.

FBF1 translocates from primary cilia to PML-NBs upon senescence induction

CEP164, another TF component, was previously reported to localize in nuclear DNA damage foci in IR-treated human RPE cells, and CEP164 deficiency in Zebrafish leads to sensitivity to DNA damage[17]. To determine if FBF1 show any function correlation with CEP164, we set out to examine the subcellular localization of FBF1 during senescence progression. Surprisingly, although the ciliary localization of FBF1 show no change, endogenous FBF1 gradually translocated into the nucleus and colocalized with PML-NBs (Fig. 3a), a group of highly dynamic, proteinaceous structures with validated function linked to stress-induced responses[18]. The reported nuclear foci of CEP164 are not PML-NBs[17], suggesting FBF1 and CEP164 act in different pathways. PML-NB upregulation is well-studied hallmark for senescent cells. Super-resolution structured illumination microscopy (SIM) analysis confirmed that translocated FBF1 indeed colocalized with PML, a core component of PML-NB (Fig. 3b). Examination of isolated nuclear

and cytoplasmic proteins confirmed that FBF1 gradually entered the nucleus upon IR-treatment (Supplementary Fig. 3a). Strikingly, ablation of *FBF1* completely suppressed PML-NB upregulation in IR-treated IMR-90 cells (Fig. 3c) or RCTE cells (Supplementary Fig. 3b). In contrast, FBF1 overexpression significantly upregulated PML-NBs in IR-treated cells (Supplementary Fig. 3c). In agreement with the critical role of cilia in senescence regulation, PML-NB translocation of FBF1 was suppressed in *IFT88*-knockdown IMR-90 cells (Supplementary Fig. 3d).

Deficiency of ARL3 or ARL13B promotes IR-induced PML-NB translocation of FBF1

The intriguing fact that three ciliary proteins, ARL3, ARL13B and FBF1, act as key negative or positive regulators of senescence suggests that the primary cilium might be an overlooked organelle critical for senescence regulation, and potential functional crosstalk between the ciliary ARLs and FBF1. Intriguingly, deficiency of *ARL3* or *ARL13B* strongly promoted PML-NB translocation of FBF1 and PML-NB upregulation in IR-treated IMR-90 or RCTE cells (Fig. 3d and Supplementary Fig. 3e), suggesting that the ciliary ARLs and FBF1 functionally converge through a PML-NB-dependent manner to regulate senescence.

IR induces FBF1-UBC9 association and FBF1 SUMOylation

A distinct feature of PML-NBs is the recruiting of SUMOylated proteins[8]. We previously discovered that UBC9, the sole E2 SUMO-conjugating enzyme, associates with and SUMOylates ARL13B in the cilia of renal epithelial cells[19]. However, we did not detect ARL13B or ARL3 translocation into the nucleus in IR-treated cells. Since FBF1 translocates to PML-NBs in senescent cells, we examined if FBF1 could be SUMOylated. *in-vitro* SUMOylation assay detected strong SUMOylation in the FBF1 C-terminal fragment (Fig. 4a). Immunoprecipitation (IP) assay further confirmed endogenous association between FBF1 and UBC9 and FBF1 SUMOylation, which increased greatly upon IR treatment (Fig. 4b, c and Supplementary Fig. 4a).

The ARL13B-ARL3 GTPase cascade inhibits UBC9-mediated FBF1 SUMOylation

We then determined how ciliary ARLs contributes to IR-induced FBF1 SUMOylation. Intriguingly, endogenous ARL3 was associated with UBC9 in non-senescent cells (Fig. 4d). Purified GST-ARL3 interacted with His-UBC9 *in vitro* (Fig. 4e). *ARL3* deficiency significantly promoted FBF1-

UBC9 interaction and IR-induced FBF1 SUMOylation (Fig. 4f, g), whereas ARL3 overexpression impaired the FBF1-UBC9 interaction (Fig. 4h). Purified His-ARL3 compromised the FBF1-UBC9 interaction (Fig. 4i) and reduced FBF1 SUMOylation in a dose-dependent manner (Fig. 4j), suggesting that ARL3 directly competes with FBF1 for UBC9 binding. The downregulation of ARL3 upon IR treatment thus releases UBC9 to SUMOylate FBF1.

Both ARL13B and ARL3 act as negative senescence regulators. Our previous discovery that ARL13B serves as a GEF to activate ARL3 suggests that ARL3 regulation of FBF1 SUMOylation may depend on its GTPase activity. To test this hypothesis, we overexpressed WT (wildtype), GTP-lock (dominant active, DA) or GDP-lock (dominant negative, DN) variants of ARL3 in RCTE cells. In agreement with our hypothesis, the $ARL3^{DA}$ variant showed stronger interaction with UBC9 than $ARL3^{WT}$, whereas the $ARL3^{DN}$ variant exhibited the opposite phenotype (Fig. 4k and Supplementary Fig. 4b). As expected, the FBF1-UBC9 interaction was largely attenuated in $ARL3^{DA}$-expressing cells (Fig. 4k). Similar to the results in *ARL3* knockdown cells, *ARL13B* deficiency led to increased FBF1-UBC9 association (Supplementary Fig. 4c), whereas overexpression of $ARL13B^{WT}$, but not $ARL13B^{DN}$, impairs IR-induced FBF1-UBC9 association (Supplementary Fig. 4d). Consistently, $ARL3^{DA}$-overexpressing cells were more resistant to senescence induction in IR-treated IMR-90 cells (Supplementary Fig. 4e-g).

SUMO protease SENP1 counteracts FBF1 SUMOylation and PML bodies translocation

Like most posttranslational modifications, SUMOylation is a reversible process[20]. Sentrin/SUMO-specific proteases (SENPs) catalyze the de-conjugation of SUMO[21]. We discovered that endogenous or overexpressed SENP1 strongly labels the ciliary base in non-senescent cells (Fig. 5a and Supplementary Fig. 5a). SIM studies confirmed that endogenous SENP1 labels a specific region that overlaps with FBF1 in non-senescent cells (Fig. 5b). FBF1 could coimmunoprecipitate either overexpressed or endogenous SENP1 (Fig. 5c, d). Intriguingly, IR-treatment greatly reduced the ciliary SENP1 signal, the total SENP1 level, and disrupted FBF1-SENP1 association (Fig. 5e, f). As expected, knockdown of *SENP1* drastically enhanced PML-NB translocation of FBF1 and PML-NB upregulation in IR-treated cells (Supplementary Fig. 5b). Overexpression of WT SENP1, but not a SENP1 variant that lost enzymatic activity[22], diminished UBC9-mediated FBF1 SUMOylation (Fig. 5g). To further confirm that FBF1 regulation by SENP1 is cilia-dependent, we

used a chemically inducible cilia trapping system[23]. Trapping SENP1 to the ciliary base could effectively attenuate both PML-NB translocation of FBF1 and PML-NB upregulation in IR-treated *ARL3*-deficient cells (Fig. 5h and Supplementary Fig. 5c). These data strongly suggest that removal of the ciliary SENP1 in stressed cells is crucial for ARL-regulated FBF1 SUMOylation, FBF1 PML-NB translocation, and senescence initiation.

TF localization is a prerequisite for PML-NB translation of FBF1 in stressed cells

To further distinguish if it is the ciliary or non-ciliary FBF1 responsible for initiating senescence responses, we knocked down the key TF structural components CEP83 or SCLT1. *CEP83* or *SCLT1* deficiency disrupts TFs[24]. Knockdown of either *CEP83* or *SCLT1* abolished the TF-localization of FBF1 as expected (Supplementary Fig. 6a and 7a). Remarkably, *CEP83* or *SCLT1* deficiency effectively inhibited PML-NB translocation of FBF1, PML-NB upregulation (Supplementary Fig. 6a and 7b), and senescence responses (Supplementary Fig. 6b-e and 7c-e) in IR-treated cells, strongly supporting TFs localization of FBF1 is a prerequisite for senescence initiation.

***Fbf1* ablation protects mice from IR-induced senescence and associated frailty**

Cellular senescence and its associated SASP are causally implicated in age-related pathologies and cancer in humans[1,25]. It is thus critical to understand how stressed cells initiate senescence program and to use the knowledge to develop interventions to blunt deleterious senescence and improve healthspan/lifespan. Consistent results obtained from different mammalian cell types suggest an exciting and highly conserved paradigm that primary cilia, the sensory antennae of cells, use the ARL13B-ARL3-UBC9-FBF1 pathway to directly communicate with PML-NBs, the well-accepted nuclear signaling hub for stress responses, to initiate senescence program in stressed cells. To test the *in-vivo* importance of FBF1-regulated senescence, we subjected *Fbf1*$^{tm1a/tm1a}$ mice to a sublethal dose of total-body IR treatment as described[26]. Strikingly, after IR-treatment, WT but not *Fbf1*$^{tm1a/tm1a}$ mice showed accelerated aging phenotypes with massive hair greying and decreased body weight (Fig. 6a, b and Supplementary Fig. 8a,). Immunohistochemistry also showed that p16^{INK4a} and IL1α accumulation in the liver of WT but not *Fbf1*$^{tm1a/tm1a}$ mice (Fig. 6c). Analysis of senescence and SASP markers indicated senescence responses were strongly induced in the vital organs of WT, but not *Fbf1*$^{tm1a/tm1a}$ mice 2 weeks after IR-treatment (Fig. 6d-g, and Supplementary

Fig. 8b, c). To determine if *Fbf1* ablation protects animals from IR-associated long-term frailty, we measured muscle strength and physical endurance in animals 6 months after IR-treatment. Of note, *Fbf1*$^{tm1a/tm1a}$ mice are healthy obese[16]. The increased body weight of *Fbf1*$^{tm1a/tm1a}$ mice may explain their reduced performance in RotaRod and treadmill even in non-IR-treated group (Fig. 6h, j). Nonetheless, only WT, but not *Fbf1*$^{tm1a/tm1a}$, mice exhibited deteriorated healthspan 6 months after IR-treatment (Fig. 6h-j).

Discussion

Here we reveal a paradigm that the suppression of a ciliary ARL13B-ARL3 GTPase cascade in stressed cells promotes the cilium-to-PML-NB translocation of FBF1, a decisive molecular event to drive senescence initiation (schematically shown in Fig. 5i). Genetic ablation of *Fbf1* effectively blocked IR-induced senescence responses and suppressed long-term healthspan decline. Emerging evidence highlights the promising potential to target cellular senescence in treating age-related diseases and even cancer[5,27]. Our discoveries assign primary cilia a central role in senescence initiation and highlight primary cilia of stressed cells as promising targets to dampen deleterious senescence and improve healthspan/lifespan.

PML-NBs are highly dynamic and functional heterogeneity[8,28]. Although a small number of core proteins define the PML-NB (e.g., PML, DAXX, SP100, SUMO), hundreds of other proteins localize to PML-NBs in dynamic fashion, and certain PML-NB components undergo continuous exchange with the surrounding nucleoplasm[7,8]. Understanding the dynamic sequestration and function of PML-NB components, especially in stressed cells, is thus critical for understanding how PML-NBs carry out multifaceted stress-induced functions. The persistent colocalization of FBF1 and PML-NBs in stressed cells suggests that, like PML protein, FBF1 may shake hands with diverse interactors in different stages of senescence. At the ciliary base, FBF1 occupies the space between transition fibers[29], and forms a proteinaceous matrix-like barrier implicated in selective protein exchange[30-32]. It is tempting to speculate that FBF1 plays a conserved role to forms a matrix-like architecture on the surface of stress-induced PML-NBs and regulates the dynamic recruitment/exchange of diverse senescence effectors/regulators in stressed cells.

There have been contradictory observations that cilia either exist[33] or are absent[34] in senescent cells. Our discovery that primary cilia only form transiently during senescence progression highlights a delicate strategy used in stressed cells by licensing ciliogenesis program to authorize the ARL-UBC9-FBF1 pathway after sensing irreparable damages. This combination likely allows irreversible senescence to be precisely controlled. Thus, primary cilia should not be considered static but rather dynamic structures sensing and transducing irreparable cues at the right time. Controlled ciliogenesis can serve as a safe mechanism for senescence induction. It appears that the downregulation of the ciliary ARLs, from regulation of transcription/translation and/or protein

stability, is enough to induce senescence by releasing UBC9 and promoting FBF1 SUMOylation, a process might be independent of sensory function of the primary cilium. However, whether and how primary cilia of stressed cells can sense irreparable damage still remains an intriguing question. Cilia/flagella emerged in single-cell eukaryote organisms and evolved as sensory devices before the appearance of senescence programs in more sophisticated organisms. It remains plausible that sensory function of primary cilia could be hijacked by stressed cells to sense stress cues, such as SASP components released autocrinally or paracrinally, to initiate senescence responses. Several studies indeed correlated cilia with SASP components in mammalian cells. For example, ciliogenesis of mesenchymal stromal cell is regulated by tumor necrosis factor-α[35]. IL-6 receptor IL-6Rα is restricted to primary cilia of epithelial cells[36]. To this end, determination of the repertoire and function of sensory receptors in the cilia of stressed cells holds great promise for deeper insights central to senescence regulation.

Methods

Animals

All animal experiments were performed according to protocols approved by the Institutional Animal Care and Use Committee (IACUC) at the Mayo Clinic (protocol A00053215–15). C57BL/6J mice were purchased from the Jackson Laboratory. The *Fbf1*$^{tm1a/tm1a}$ mice were obtained from Trust Sanger Institute and refreshed the genetic background as described[16]. The *Arl3* floxed mouse line was a gift from Dr. Wolfgang Baehr's lab[37]. Mice were maintained in a pathogen-free facility at 23–24 °C under a 12 h light-dark cycle regimen with free access to a NCD (standard mouse diet Lab Diet 5053, St. Louis, MO) and water. Mice were bred and housed under a Specific Pathogen-Free (SPF) status. All mice were housed in static autoclaved HEPA-ventilated microisolator cages (27 × 16.5 × 15.5 cm) with autoclaved Enrich-o'Cobs (The Andersons Incorporated) for bedding. Cages and bedding were changed biweekly. Cages were opened only in class II biosafety cabinets. The majority of subjects from the study are the result of in-house mating, and littermate controls were used. Both male and female mice were used for the study, and the age was indicated in the figure legends.

Tissues from mice sacrificed at the indicated time points were snap-frozen in liquid nitrogen for biochemical studies or fixed in 4% paraformaldehyde for 24 hours prior to processing and paraffin embedding. Paraffin-embedded tissues were cut into 5-μm sections.

Cells and cell culture

IMR-90, RCTE and HEK293T cells were purchased from ATCC. IMR-90 cells were cultured in EMEM (Eagle's minimum essential medium). RCTE cells were cultured in DMEM/F12. HEK293T cells were cultured in DMEM. The medium was supplemented with 10% fetal bovine serum and 1% penicillin and streptomycin. Cells were cultured under 5% CO2 and 5% O2 at 37°C. MEFs were generated by standard methods as described previously[16]. Briefly, MEFs were generated from embryonic day 13.5 (E13.5) embryos of WT and mutant mice under the normal culture condition that includes DMEM with 10% FBS and 5% CO2.

Senescence and SA-β-Gal assays

Senescence was induced by irradiation. For ionizing radiation experiments, IMR-90 cells were exposed with 10 Gy by the X-ray irradiator (RS-2000 X-ray irradiator). RCTE or MEF cells were irradiated with 5 or 12 Gy X rays, respectively. The cells were harvested and analyzed 10 days

later or otherwise indicated time. Control (proliferating) cells were mock irradiated. Senescent cells were identified by a senescence-associated β-galactosidase kit (Cell signaling) according to the manufacturer's protocol.

Stable cell lines

Stable cell lines were constructed using lentivirus system. For producing lentiviral particles, pCDH or pLKO.1 construct, together with psPAX2 (Addgene #12260) and pMD2.G (Addgene #12259), was transfected into HEK293T cells using Fugene6 (Promega). Medium was replaced after 24 h, and virus was harvested 48 h post-transfection. Virus was filtered with a 0.45-μm OVDF filter (Millipore) and concentrated using Lenti-X Concentrator (Takara). Then, target cells were infected by lentivirus overnight with 10 μg/mL polybrene (Millipore), and medium was replaced. The cells were further selected by puromycin or G418 at 48 h after post-infection and fed with fresh puromycin or G418 every 2 days.

Immunofluorescence microscopy

For FBF1 and PML-NB staining, cells were grown on glass coverslips and fixed with −20 °C methanol for 20 min, then blocked with 3% BSA and immune-stained with appropriate antibodies. For cilia staining, cells were fixed with 4% paraformaldehyde for 20 min at room temperature, followed by permeabilization with 0.1% Triton X-100 for 10 min. Cells were then blocked with 3% BSA and immune-stained with appropriate antibodies. Fluorescence images were acquired using Nikon TE2000-U with Metamorph software (Molecular Devices).

Antibodies

ARL13B (17711-1-AP; dilution 1:2000 for immunofluorescent and 1:1000 for western blotting), FBF1 (11531-1-AP; dilution 1:1000 for immunofluorescent and western blotting), ARL3 (10961-1-AP; dilution 1:1000 for immunofluorescent and western blotting), p16INK4a (10883-1-AP; dilution 1:1000 for western blotting), CEP83 (26013-1-AP; dilution 1:1000 for immunofluorescent and western blotting), SCLT1 (14875-1-AP; dilution 1:1000 for immunofluorescent and western blotting), IL6 (66146-1-Ig; dilution 1:1000 for western blotting), IL1α (16765-1-AP; dilution 1:200 for immunohistochemistry) from Proteintech; p16INK4a (ab54210; dilution 1:200 for immunohistochemistry) from Abcam; p16INK4a (SPC-775D; dilution 1:500 for western blotting) from StressMarq Biosciences; acetylated tubulin (T7451, dilution 1:5000 for immunofluorescent), β-actin (A1978; dilution 1:2000 for western blotting), FLAG tag (F1804; dilution 1:2000 for

western blotting), HA tag (H3663; dilution 1:2000 for western blotting) and Myc tag (SAB2702192; dilution 1:2000 for western blotting) from Sigma; p21 (sc-6246; dilution 1:500 for western blotting), PML (sc-966; dilution 1:500 for immunofluorescent), SENP1 (sc-271360; dilution 1:500 for immunofluorescent and western blotting)from Santa Cruz; ac-p53 (2525; dilution 1:1000 for western blotting) from Cell Signaling technology.

DNA constructs and siRNAs

Human FBF1, SENP1, ARL3^{WT}, ARL3^{DA} and ARL3^{DN} were generated by PCR and subcloned into pCDH-Myc vector. CFP-FRB-CEP170c, YFP-FKBP12 and YFP-FKBP12-SENP1 were subcloned into pCDH vector. Human SUMO1, UBC9, SENP1 and SENP1 C603S were subcloned into pcDNA3-HA or pcDNA3-Flag vectors to generate HA-SUMO1, Flag-UBC9, Flag-SENP1 and Flag-SENP1 C603S constructs. Human FBF1 (598-1148 domain), ARL3 and UBC9 fragments were inserted into pET4T1 or pET28a vectors to generate GST-FBF1-CT, GST-ARL3, His-ARL3 or His-UBC9 plasmids, respectively. All constructs were verified by DNA sequencing. For construction of knockdown stable cell lines, shRNAs were inserted into pLKO.1-TRC plasmid, according to the Addgene instructions. siRNA duplexes were introduced into cells with Lipofectamine RNAiMAX (Invitrogen), following the manufacturer's manual. Typically, after siRNA transfection, cells were collected for further analysis by western blot or immunofluorescence microscopy at the indicated time. RNAi Negative Control was purchased from GE Healthcare Dharmacon. siRNA oligonucleotides were obtained from Invitrogen. Sequences of shRNA or siRNA targeting corresponding mRNAs used are listed in Table S2.

CRISPR-Cas9 gene editing

ARL3, ARL13B and FBF1 guide RNA (gRNA) was designed using an online tool (https://zlab.bio/guide-design-resources) and subcloned into pSpCas9(BB)-2A-GFP (px458), in which a green fluorescent protein (GFP) was fused to Cas9. RCTE cells were transfected with the gRNA construct for 48 h and then subjected to flow cytometry to sort single GFP-positive cells. Single clones were expanded for further confirmation of the on-target cleavage using genomic PCR, followed by Sanger sequencing. gRNA sequences used are listed in Table S2.

Immunoprecipitation assay and GST pull-down assay

Immunoprecipitation was performed using HEK293T or RCTE cell lysate in IP buffer (25 mM Tris-HCl, pH 7.4, 10 mM KCl, 1.5 mM $MgCl_2$, 1 mM EDTA, 1 mM EGTA, 150 mM NaCl, 0.5%

NP-40), with complete protease inhibitor cocktail (Roche) added, following the manufacturer's manuals. The supernatant was collected by centrifugation for 20 min at 12,000g at 4 °C and further pre-cleared using protein-G Sepharose for 4 h. After removal of protein-G beads, the pre-cleared supernatant was incubated with protein-G beads and 2 μg of the indicated primary antibodies or IgG control overnight at 4 °C. After washing, the Sepharose beads were boiled in 1×SDS-PAGE loading buffer. Proteins were detected by western blotting. For GST pull-down assays, GST, the GST-fusion protein of FBF1 (C terminal) and 6× his-tagged UBC9 proteins were expressed in *Escherichia coli* BL21 strain and purified using glutathione or His resin Sepharose. Purified His-UBC9 proteins were incubated with GST or the GST-fusion proteins immobilized on glutathione Sepharose in binding buffer (25 mM Tris-HCl, pH 7.4, 150 mM NaCl, 1 mM EDTA, 10% glycerol, and 0.5% Triton X-100 and protease inhibitors) at 4 °C for 4 h. The beads were then washed with binding buffer and eluted in 1× SDS-PAGE loading buffer for further analysis by western blotting.

Western blot

Cells or tissues were homogenized in RIPA buffer with protease inhibitors (Roche). Protein concentration in each sample was measured using the BCA Pierce Protein assay kit (ThermoFisher) and normalized to the lowest concentration. Protein samples were subjected to standard SDS-PAGE gels and transferred to immuno-blot PVDF membranes (Millipore), then blocked with 5% nonfat dry milk and incubated overnight at 4 °C with primary antibodies. The secondary antibodies anti-mouse or anti-rabbit HRP-conjugated antibodies were incubated for 1 h at room temperature. After washing with TBS-T three times for 10 min each, horseradish peroxidase (HRP) substrates (ThermoFisher) were used to develop signals. Images were obtained using ChemiDoc Touch Imaging System (BIO-RAD).

RNA isolation and qRT-PCR

For cultured cells, total RNA was extracted by TRIzol reagent (Invitrogene). cDNA was synthesized from the purified RNA using a high-capacity cDNA reverse transcription kit (Applied Biosystems). qPCR was performed using SYBR Green PCR Master Mix (BIO-RAD) with CFX384 real-time system (BIO-RAD). Tissue samples were lysed in Trizol reagent and homogenized for qRT-PCR. PCR primers used are listed in Table S1.

Immunohistochemistry

For immunohistochemistry staining, tissue sections (5 μm thickness) were deparaffinized in xylene and rehydrated through alcohol gradient, incubated with hydrogen peroxide (Dako) for 10 minutes to quench the endogenous peroxidase activity, and then rinsed with PBS three times. Antigen retrieval was performed using a steamer for 30 min in 0.1 M citrate buffer (pH 6.0). Serum-free protein block (Dako) was used to prevent nonspecific protein binding. Sections were then incubated with primary antibodies overnight at 4°C, followed by a 60-min incubation with anti-rabbit secondary antibody at room temperature. The slides were developed with DAB Peroxidase Substrate Kit (Dako), counterstained with hematoxylin, dehydrated in ethanol, cleared in xylene, and then mounted with Permount mounting medium (Thermo Fisher Scientific).

Cell viability assay

IMR-90 or MEF cells were plated as triplicates in 96-well plates and cultured for 48 h at 37°C. After treatment with X-rays for indicated time, 10 μl of 12 mM 3-(4,5-dimethylthiazol-2-yl)-2,5-diphenyltetrazolium bromide (MTT) was added to each well and incubated for another 4 h. After replacing the culture medium with Stop Solution (40 mM HCL in isopropanol; 100 μl/well), the absorbance was measured at 590 nm on a plate reader.

TUNEL assay

Apoptosis of the cells in senescence was detected with a TUNEL assay kit (DeadEnd™ Fluorometric TUNEL System, G3250, Promega) following the manufacturer's protocol.

***In-vitro* SUMOylation**

The *in-vitro* SUMOylation kit reaction was purchased from Enzo Life Sciences. The reaction contains E1 and E2 enzymes, SUMO1/2/3, and GST-FBF1 (C terminal) proteins in SUMOylation buffer. SUMOylation reactions were incubated at 30°C for 1 h. After termination with SDS-PAGE sample buffer, reaction products were subjected to SDS-PAGE.

Chemically inducible cilia trapping system

The basis of the technology is chemically inducible dimerization, in which rapamycin induces the dimerization of FKBP-rapamycin binding domain (FRB) and FK506 binding protein (FKBP). To localize a fusion protein of YFP-FKBP-SENP1 to the ciliary base, we used the C terminus of CEP170. Transfected RCTE cells were incubated with 100 nM rapamycin for 30 min and then exposed with 5Gy X-rays for 5 days. Washout of rapamycin after 30 min did not affect protein dimerization in cells owing to the irreversible nature of the system.

Total body irradiation

WT, *Fbf1*$^{tm1a/tm1a}$ C57BL/6 mice of both sexes at 6 months of age were mock-irradiated or exposed to sub-lethal total body irradiation (4.25 Gy Gamma rays), and the indicated tissue was harvested at 14 days after the procedure for IHC, western blotting or real-time PCR analysis. The physical function measurements were performed after 6 months post irradiation. Mice of both genders were randomly allocated to different groups and experiments were conducted non-blinded.

Physical function measurements

Maximal walking speed was assessed using an accelerating RotaRod system. Mice were trained on the RotaRod for 2 days at speeds of 4, 6, and 8 rpm for 300 sec. On the test day, mice were placed onto the RotaRod and then started at 4 rpm. The rotating speed was accelerated from 4 to 40 rpm over a 5-min interval. Testing consisted of three trials separated by a 30-min interval. Maximum trial length was 5 min, and results were averaged from three trials. Forelimb grip strength (N-F/kg) was determined using a Grip Strength Meter. Results were averaged over four trials. For treadmill performance, mice were first acclimated to the treadmill for 3 consecutive days for 5 min each day starting at a speed of 5 m/min for 2 min, 7 m/min for 2 min, and then 9 m/min for 1 min at a 5% grade. On the test day, mice ran on the treadmill at an initial speed of 5 m/min for 2 min, and then the speed was increased by 2 m/min every 2 min until the mice were exhausted. Exhaustion will be defined as the inability of the mouse to remain on the treadmill despite an electrical shock stimulus and mechanical prodding. Running time was recorded and running distance and work (the product of body weight [kg], gravity [9.81 m/s2], vertical speed [m/s x angle], and time [s]) were calculated.

Statistical analysis

Statistical significance was determined by unpaired Student's t test, one-way, or two-way ANOVA, accordingly. *p* values <0.05 were considered statistically significant ($*p < 0.05$; $**p < 0.01$; $***P < 0.001$)

Acknowledgments

We thank Dr. Takanari Inoue (Stanford University) for sharing cilia trapping system and Dr. Wolfgang Baehr (U. Of Utah) for sharing *Arl3*$^{flox/flox}$ mice.

Funding:

This work was supported from the National Institutes of Health (NIH) research grants R01DK090038, R01DK099160 to JH; the Department of Defense (W81XWH2010214), and Pilot and Feasibility subawards from Mayo Clinic Translational PKD Center (P30DK90728) and Baltimore PKD Center (2P30DK090868) to KL; R01AG058812 to EC; R37 AG013925, P01 AG062413, R33 AG061456, the Connor Fund, Robert J. and Theresa W. Ryan, and the Noaber Foundation to JK.

Author contributions:

J.H.H. generated the hypothesis and designed the experiments. X.Y.M., Y.Y.Z., and Q.W. conducted most experiments. Q.W. Y.Y.Z. X.Y.M., and Y.H. established and characterized the *Fbf1*$^{tm1a/tm1a}$ mice. X.Y.M., Y.Y.Z., Y.H., J.L.H., X.Z. and N.K.L. contributed to the animal studies. X.Y.M. and C.C. contributed to the immunofluorescence experiments. X.Y.M. and D.B.Z. contributed to protein purification. X.Y.M., Y.Y.Z., and K.H. contributed to the plasmid design and construction. K.L., Q.W., J.L.K. and E.N.C. contributed reagents and discussed data. X.Y.M. and J.H.H. wrote the manuscript with input from all coauthors.

Competing interests:

The authors declare no competing interests.

Data and materials availability:

All data and materials are available from the corresponding author upon reasonable request.

References

1. Gorgoulis, V. *et al.* Cellular Senescence: Defining a Path Forward. *Cell* **179**, 813-827 (2019).
2. Sharpless, N.E. & Sherr, C.J. Forging a signature of in vivo senescence. *Nature reviews. Cancer* **15**, 397-408 (2015).
3. Faget, D.V., Ren, Q. & Stewart, S.A. Unmasking senescence: context-dependent effects of SASP in cancer. *Nat Rev Cancer* **19**, 439-453 (2019).
4. He, S. & Sharpless, N.E. Senescence in Health and Disease. *Cell* **169**, 1000-1011 (2017).
5. Di Micco, R., Krizhanovsky, V., Baker, D. & d'Adda di Fagagna, F. Cellular senescence in ageing: from mechanisms to therapeutic opportunities. *Nat Rev Mol Cell Biol* **22**, 75-95 (2021).
6. Salomoni, P. & Pandolfi, P.P. The role of PML in tumor suppression. *Cell* **108**, 165-170 (2002).
7. Corpet, A. *et al.* PML nuclear bodies and chromatin dynamics: catch me if you can! *Nucleic Acids Res* **48**, 11890-11912 (2020).
8. Bernardi, R. & Pandolfi, P.P. Structure, dynamics and functions of promyelocytic leukaemia nuclear bodies. *Nat Rev Mol Cell Biol* **8**, 1006-1016 (2007).
9. Singla, V. & Reiter, J.F. The primary cilium as the cell's antenna: signaling at a sensory organelle. *Science* **313**, 629-633 (2006).
10. Goetz, S.C. & Anderson, K.V. The primary cilium: a signalling centre during vertebrate development. *Nat Rev Genet* **11**, 331-344 (2010).
11. Cantagrel, V. *et al.* Mutations in the cilia gene ARL13B lead to the classical form of Joubert syndrome. *Am J Hum Genet* **83**, 170-179 (2008).
12. Alkanderi, S. *et al.* ARL3 Mutations Cause Joubert Syndrome by Disrupting Ciliary Protein Composition. *Am J Hum Genet* **103**, 612-620 (2018).
13. Gotthardt, K. *et al.* A G-protein activation cascade from Arl13B to Arl3 and implications for ciliary targeting of lipidated proteins. *Elife* **4** (2015).
14. Zhang, Q. *et al.* GTP-binding of ARL-3 is activated by ARL-13 as a GEF and stabilized by UNC-119. *Sci Rep* **6**, 24534 (2016).
15. Wei, Q. *et al.* Transition fibre protein FBF1 is required for the ciliary entry of assembled intraflagellar transport complexes. *Nat Commun* **4**, 2750 (2013).

16. Zhang, Y. *et al.* FBF1 deficiency promotes beiging and healthy expansion of white adipose tissue. *Cell reports* **36**, 109481 (2021).
17. Chaki, M. *et al.* Exome capture reveals ZNF423 and CEP164 mutations, linking renal ciliopathies to DNA damage response signaling. *Cell* **150**, 533-548 (2012).
18. Pearson, M. *et al.* PML regulates p53 acetylation and premature senescence induced by oncogenic Ras. *Nature* **406**, 207-210 (2000).
19. Li, Y. *et al.* SUMOylation of the small GTPase ARL-13 promotes ciliary targeting of sensory receptors. *J Cell Biol* **199**, 589-598 (2012).
20. Flotho, A. & Melchior, F. Sumoylation: a regulatory protein modification in health and disease. *Annu Rev Biochem* **82**, 357-385 (2013).
21. Hickey, C.M., Wilson, N.R. & Hochstrasser, M. Function and regulation of SUMO proteases. *Nat Rev Mol Cell Biol* **13**, 755-766 (2012).
22. Xu, Z. *et al.* Crystal structure of the SENP1 mutant C603S-SUMO complex reveals the hydrolytic mechanism of SUMO-specific protease. *Biochem J* **398**, 345-352 (2006).
23. Lin, Y.C. *et al.* Chemically inducible diffusion trap at cilia reveals molecular sieve-like barrier. *Nat Chem Biol* **9**, 437-+ (2013).
24. Tanos, B.E. *et al.* Centriole distal appendages promote membrane docking, leading to cilia initiation. *Genes Dev* **27**, 163-168 (2013).
25. Pignolo, R.J., Passos, J.F., Khosla, S., Tchkonia, T. & Kirkland, J.L. Reducing Senescent Cell Burden in Aging and Disease. *Trends in molecular medicine* **26**, 630-638 (2020).
26. Dou, Z. *et al.* Cytoplasmic chromatin triggers inflammation in senescence and cancer. *Nature* **550**, 402-406 (2017).
27. Lee, S. & Schmitt, C.A. The dynamic nature of senescence in cancer. *Nat Cell Biol* **21**, 94-101 (2019).
28. Lallemand-Breitenbach, V. & de The, H. PML nuclear bodies. *Cold Spring Harb Perspect Biol* **2**, a000661 (2010).
29. Yang, T.T. *et al.* Super-resolution architecture of mammalian centriole distal appendages reveals distinct blade and matrix functional components. *Nat Commun* **9**, 2023 (2018).
30. Wei, Q. *et al.* The hydrolethalus syndrome protein HYLS-1 regulates formation of the ciliary gate. *Nat Commun* **7**, 12437 (2016).
31. Wei, Q. *et al.* Transition fibre protein FBF1 is required for the ciliary entry of assembled

intraflagellar transport complexes. *Nature communications* **4**, 2750 (2013).

32. Wei, Q., Ling, K. & Hu, J. The essential roles of transition fibers in the context of cilia. *Current opinion in cell biology* **35**, 98-105 (2015).
33. Breslin, L., Prosser, S.L., Cuffe, S. & Morrison, C.G. Ciliary abnormalities in senescent human fibroblasts impair proliferative capacity. *Cell Cycle* **13**, 2773-2779 (2014).
34. Carroll, B. *et al.* Persistent mTORC1 signaling in cell senescence results from defects in amino acid and growth factor sensing. *J Cell Biol* **216**, 1949-1957 (2017).
35. Vezina, A., Vaillancourt-Jean, E., Albarao, S. & Annabi, B. Mesenchymal stromal cell ciliogenesis is abrogated in response to tumor necrosis factor-alpha and requires NF-kappaB signaling. *Cancer Lett* **345**, 100-105 (2014).
36. Shao, R. *et al.* Downregulation of cilia-localized Il-6R alpha by 17beta-estradiol in mouse and human fallopian tubes. *Am J Physiol Cell Physiol* **297**, C140-151 (2009).
37. Hanke-Gogokhia, C. *et al.* Arf-like Protein 3 (ARL3) Regulates Protein Trafficking and Ciliogenesis in Mouse Photoreceptors. *J Biol Chem* **291**, 7142-7155 (2016).
38. Joo, K. *et al.* CCDC41 is required for ciliary vesicle docking to the mother centriole. *P Natl Acad Sci USA* **110**, 5987-5992 (2013).
39. Kurtulmus, B. *et al.* LRRC45 contributes to early steps of axoneme extension. *J Cell Sci* **131** (2018).
40. Cheng, J., Kang, X.L., Zhang, S. & Yeh, E.T.H. SUMO-Specific protease 1 is essential for stabilization of HIF1 alpha during hypoxia. *Cell* **131**, 584-595 (2007).

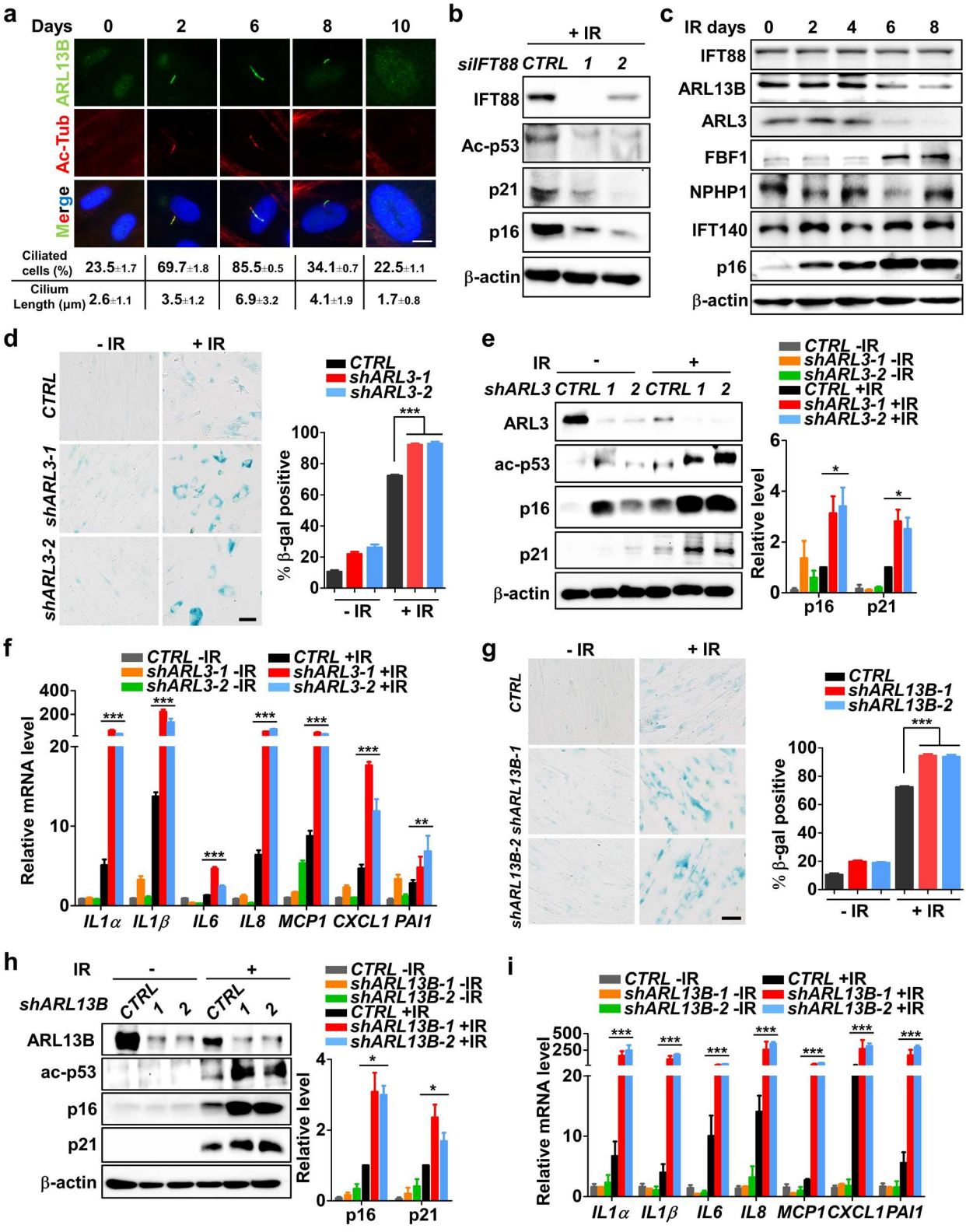

Fig. 1. Deficiency of Joubert syndrome GTPase ARL3 or ARL13B promotes DNA damage-induced senescence. a, Immunofluorescent images for changes of primary cilia in IMR-90 cells

after senescence-induction by 10 Gy X-ray's irradiation. Cilia were labeled with acetylated tubulin. Scale bar, 10 μm. **b,** Western blot of senescence markers in control or *IFT88*-knockdown IMR-90 cells at day 10 after irradiation. **c,** Western blot showing changes in ciliary protein levels after senescence-induction in IMR-90 cells by 10 Gy X-ray's irradiation. **d-f,** SA-β-gal staining (**d**), western blot of senescence markers (**e**) and relative mRNA levels of SASP markers (**f**) in IMR-90 cells stably expressing control shRNA or sh*ARL3* at day 10 after irradiation with 10 Gy X-rays. **g-i,** SA-β-gal staining (**g**), western blot of senescence markers (**h**) and relative mRNA levels of SASP markers (**i**) in IMR-90 cells stably expressing control shRNA or sh*ARL13B* at day 10 post-irradiation. Scale bar, 200 μm. Values are expressed as means ± SEMs. *$p < 0.05$, **$p < 0.01$, ***$p < 0.001$.

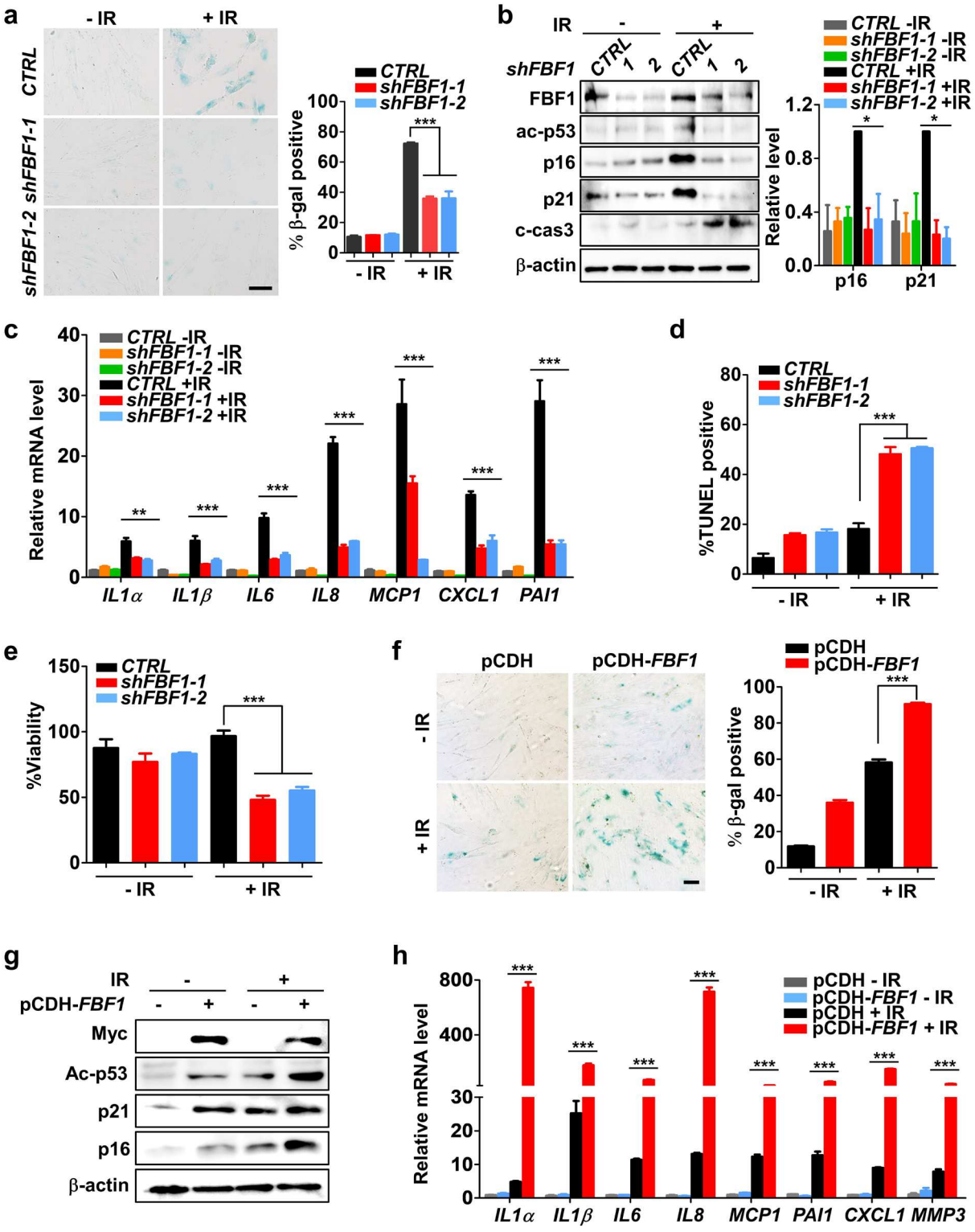

Fig. 2. Transition fiber component FBF1 is a key player in DNA damage-induced senescence. **a-c,** SA-β-gal staining (**a**), western blot of senescence markers (**b**) and relative mRNA levels of SASP markers (**c**) in IMR-90 cells stably expressing control shRNA or sh*FBF1* at day 10 post-

irradiation. Scale bar, 200 μm. **d, e,** TUNEL assay (**d**) and viability assay (**e**) in IMR-90 cells stably expressing control shRNA or sh*FBF1* at day 3 post-irradiation. **f-h,** SA-β-gal staining (**f**), western blot of senescence markers (**g**) and relative mRNA levels of SASP markers (**h**) in IMR-90 cells overexpressed with plasmid pCDH vector or pCDH-FBF1-Myc at day 7 after irradiation. Scale bar, 200 μm. Values are expressed as means ± SEMs. *$p < 0.05$, **$p < 0.01$, ***$p < 0.001$.

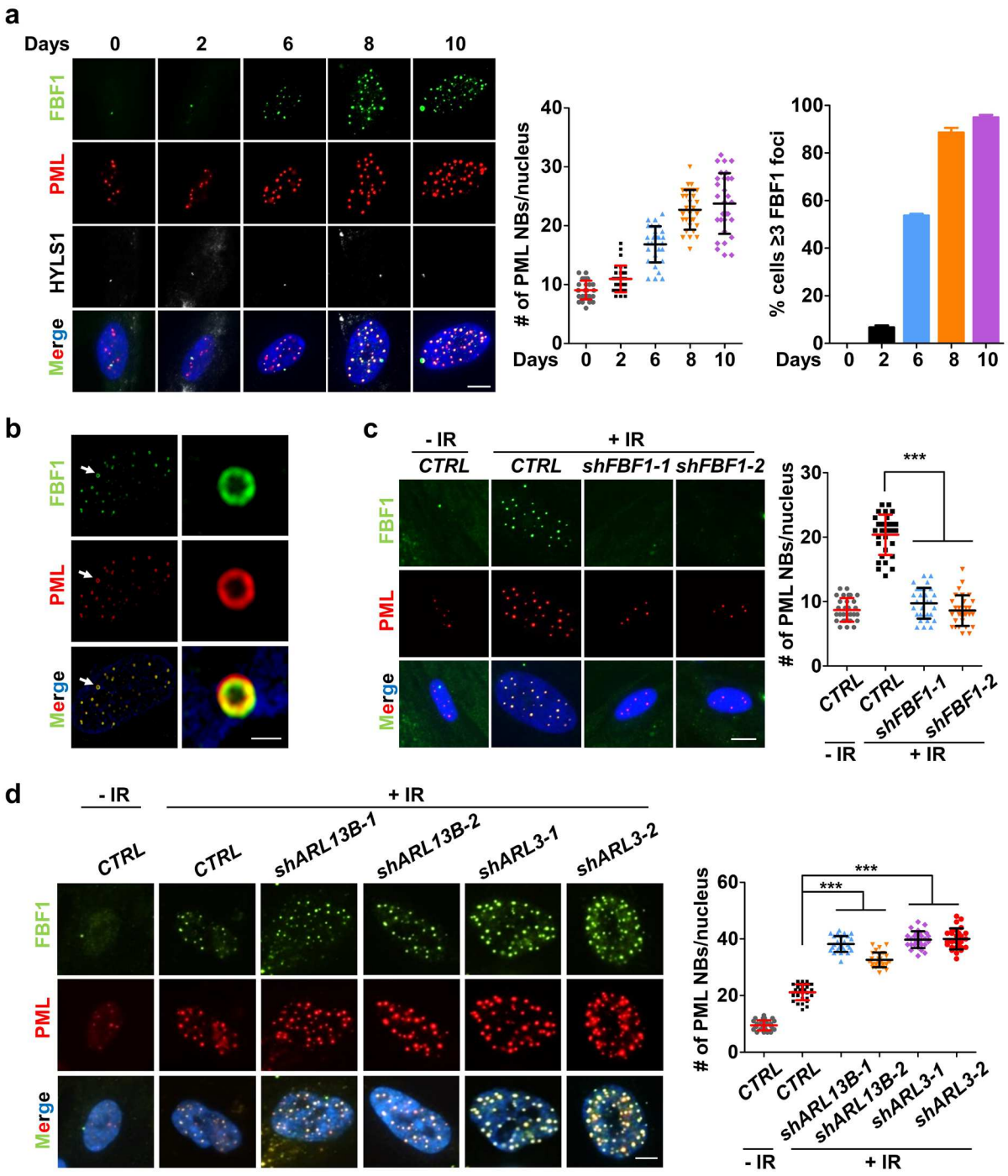

Fig. 3. ARL13B and ARL3 negatively regulate DNA damage–induced PML-NB translocation of FBF1, a prerequisite for stress-induced PML-NB upregulation. a, Immunofluorescent images in IMR-90 cells after irradiation using antibodies against FBF1 and PML. Basal bodies were labeled with HYLS1. Scale bar, 10 μm. Number of PML NBs per nucleus

and percentage of cells containing ≥3 FBF1 foci after irradiation were quantified. **b,** Structured illumination microscopic images of the nucleus of a senescent IMR-90 cell stained for FBF1 and PML. Scale bar, 2 μm. **c,** Localization of FBF1 and PML in control or *FBF1*-knockdown IMR-90 cells after irradiation. Scale bar, 10 μm. **d,** Localization of FBF1 and PML in control, *ARL3*-knockdown, or *ARL13B*-knockdown IMR-90 cells after irradiation. Scale bar, 10 μm. Values are expressed as means ± SEMs. ***$p < 0.001$.

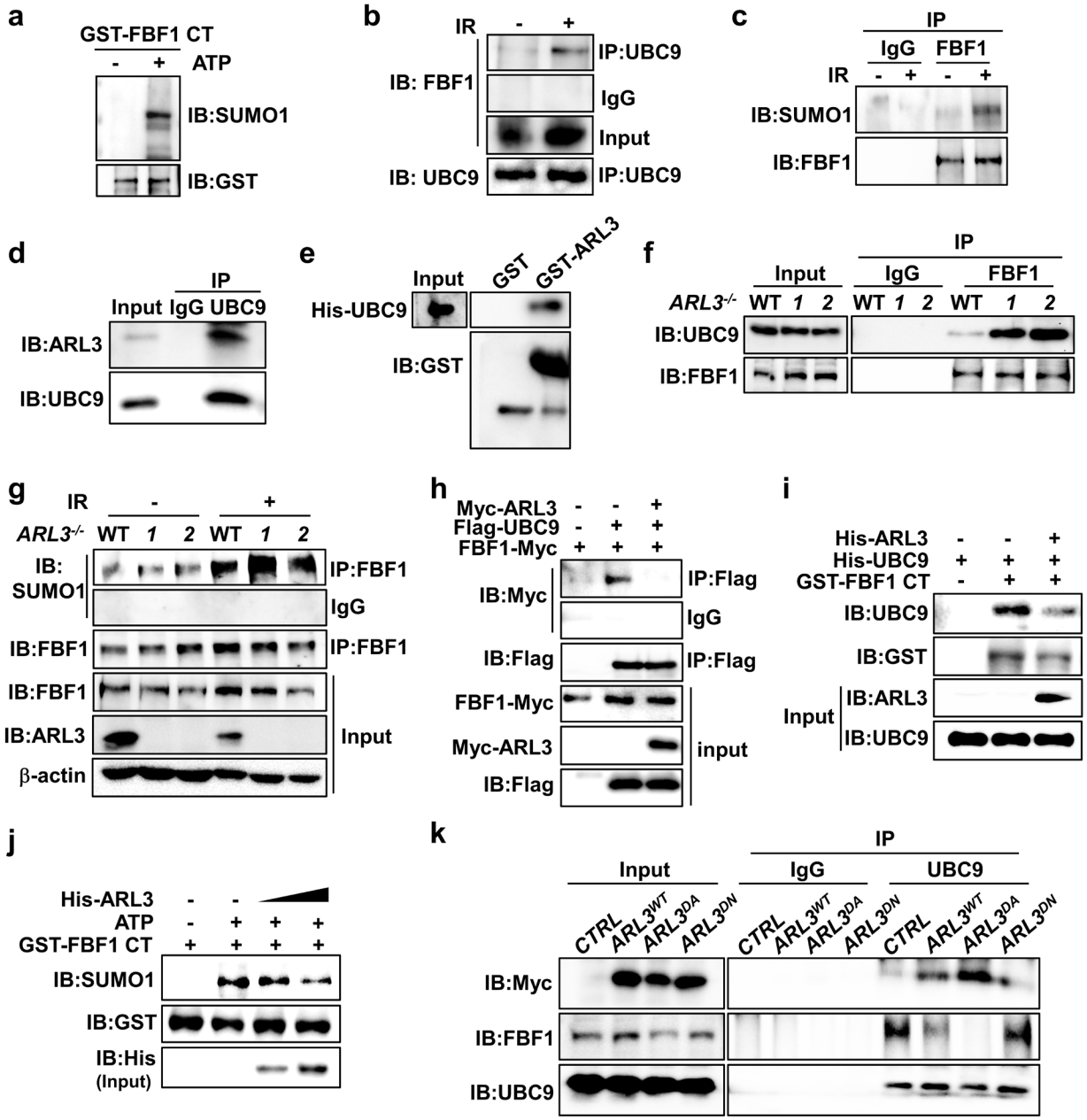

Fig. 4. DNA damage induces FBF1-UBC9 association and FBF1 SUMOylation, which are negatively regulated by the ARL13B-ARL3 GTPase cascade. a, *In-vitro* SUMOylation assay of FBF1 and western blotting using a SUMO1 antibody. GST tagged 598–1148 domain FBF1 was purified using *E. coli*. **b,** Endogenous UBC9 immunoprecipitates with FBF1 in RCTE cells after irradiation. **c,** Endogenous FBF1 immunoprecipitates with SUMO1 in RCTE cells after irradiation. **d,** Endogenous UBC9 immunoprecipitates with ARL3 in RCTE cells. **e,** GST pull-down assay

shows the ARL3 and UBC9 interaction. **f,** Endogenous FBF1 immunoprecipitates with UBC9 in WT or *ARL3*$^{-/-}$ RCTE cells with 5 Gy X-rays for 7 days. **g,** Endogenous FBF1 immunoprecipitates with SUMO1 in WT or *ARL3*$^{-/-}$ RCTE cells with or without X-rays. **h,** ARL3 inhibited the interaction between FBF1 and UBC9 by co-immunoprecipitation in 293T cells. **i,** ARL3 reduced the interaction between FBF1 and UBC9 by GST pull-down assay. GST-tagged 598–1148 domain FBF1, His-ARL3 and His-UBC9 were purified using *E. coli.* **j,** *In-vitro* SUMOylation assay was performed in a reaction with GST tagged 598–1148 domain FBF1 and His-ARL3 purified in *E. coli*. Western blotting was detected by SUMO1, GST and His antibody. **k,** Endogenous UBC9 immunoprecipitates with Myc-ARL3 or FBF1 in ARL3^{WT}, ARL3^{DA} or ARL3^{DN} overexpression RCTE cells with 5 Gy X-rays for 7 days.

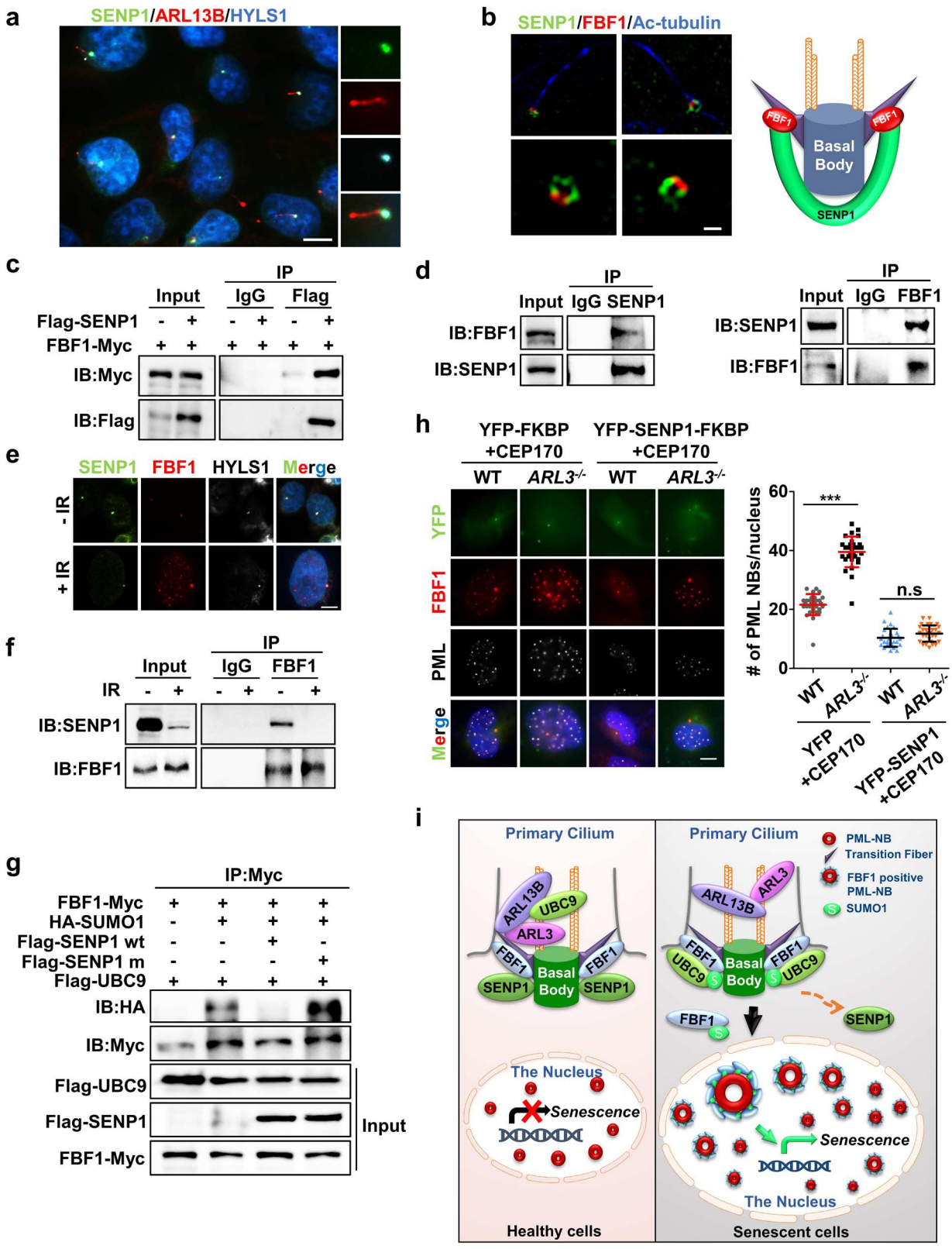

Fig. 5. DNA damage abolishes the ciliary SUMO protease SENP1 and enhances FBF1

SUMOylation. a, Immunofluorescent images for SENP1 staining in RCTE cells. Basal bodies were labeled with HYLS1. Scale bar, 10 μm. **b,** Structured illumination microscopic images stained for FBF1 and SENP1 at ciliary base in IMR-90 cells. Scale bar, 1 μm. **c,** Co-immunoprecipitation of SENP1 and FBF1 in 293T cells. **d,** Endogenous SENP1 or FBF1 immunoprecipitates with FBF1 or SENP1 in RCTE cells. **e,** Immunofluorescent images in RCTE cells without or with irradiation using antibodies against SENP1 and FBF1. Basal bodies were labeled with HYLS1. Scale bar, 10 μm. **f,** Endogenous FBF1 immunoprecipitates with SENP1 in RCTE cells with or without X-rays. **g,** SENP1 diminished FBF1 SUMOylation in a co-immunoprecipitation assay in 293T cells. **h,** Immunofluorescent images for FBF1, PML and YFP in WT or *ARL3*$^{-/-}$ RCTE cells co-transfected with CFP-FRB-CEP170c and YFP-FKBP-SENP1 plasmids after X-rays. Scale bar, 10 μm. **i,** Proposed model: DNA-damage stress strongly downregulates ARLs, enables FBF1-UBC9 interaction, and results in FBF1 SUMOylation. SUMOylated FBF1 translocates from the ciliary base to PML-NBs, which is required for stress-induced PML-NB upregulation and senescence initiation. Values are expressed as means ± SEMs. ***$p < 0.001$.

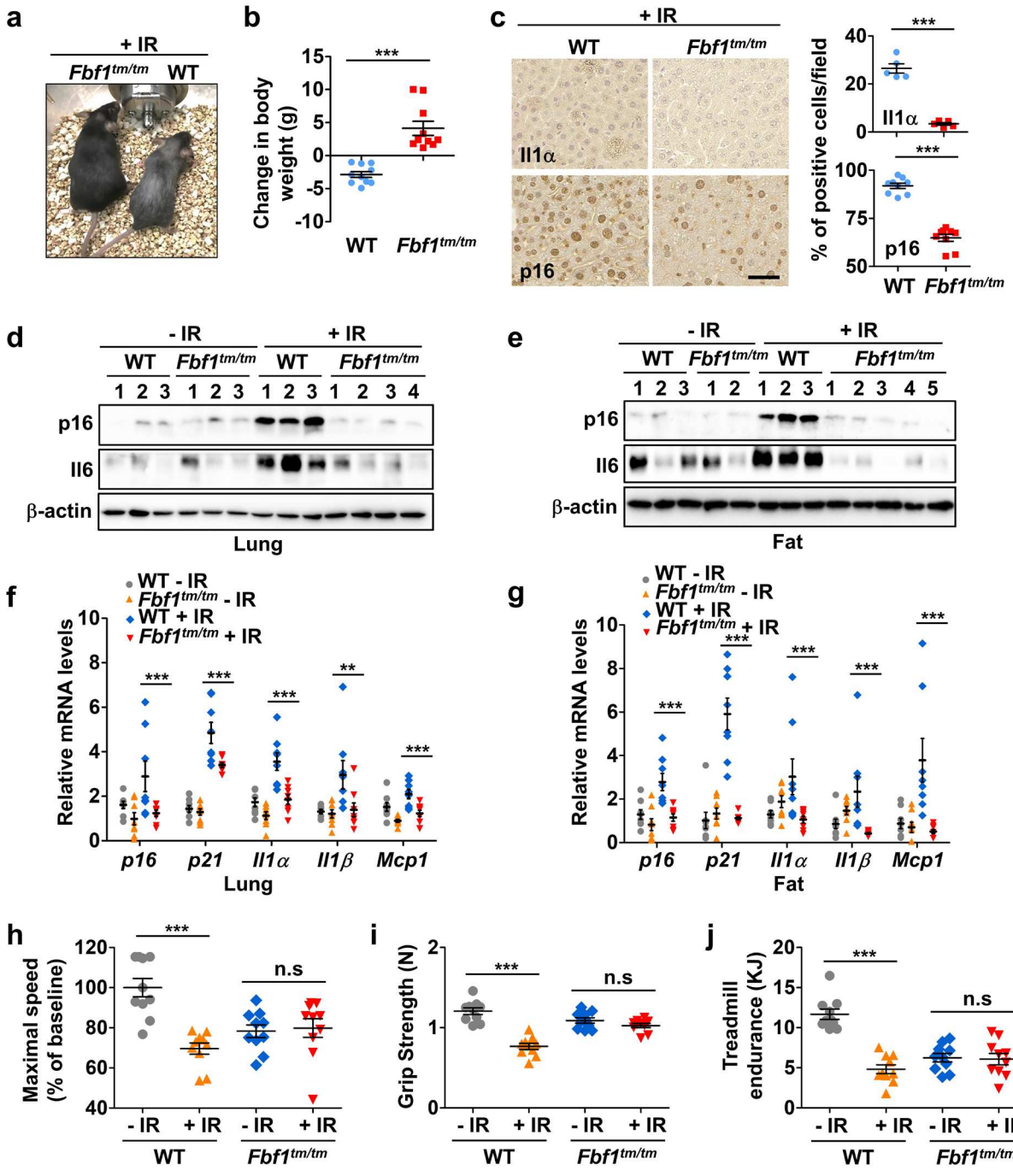

Fig. 6. *Fbf1* ablation protects mice from IR-induced senescence and associated frailty. a, Representative images of mice 3 months after IR. **b,** The change in body weight of mice with 3 months after IR. $n = 10$ mice. **c,** at 2 weeks after IR, liver was analyzed by immunohistochemistry and quantified; Scale bar: 200 μm. **d, e,** Lysates obtained from lung (**d**) and fat (**e**) tissue of WT mice, or *Fbf1*$^{tm1a/tm1a}$ mice 2 weeks after IR were analyzed for the indicated proteins by western

blot. **f, g,** SASP-related genes were assessed by RT-qPCR in extracts of lung (**f**) and fat (**g**) tissue of WT mice or *Fbf1*$^{tm1a/tm1a}$ mice 2 weeks after IR. **h-j,** Maximal speed (**h**), grip strength (**i**) and treadmill endurance (**j**) of 12-month-old WT mice or *Fbf1*$^{tm1a/tm1a}$ C57BL/6 mice, 6 months after exposure to mock or sublethal dose of total-body IR (n = 8 for both groups). Values are expressed as means ± SEMs. $^{**}p < 0.01$, $^{***}p < 0.001$.

Supplementary Files

This is a list of supplementary files associated with this preprint. Click to download.

- SupplementaryInformation.pdf